ADVANCED TOPICS IN SCIENCE AND TECHNOLOGY IN CHINA

Tingyun Kuang
Congming Lu
Lixin Zhang *Editors*

Photosynthesis Research for Food, Fuel and the Future

15th International Conference on Photosynthesis

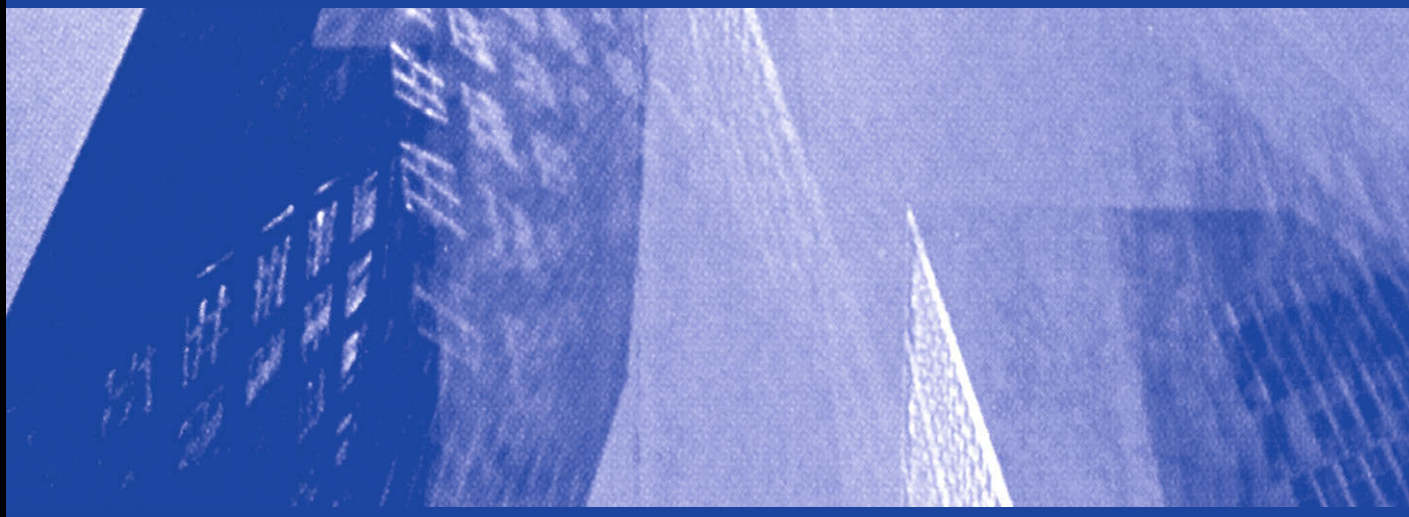

ZHEJIANG UNIVERSITY PRESS
浙江大学出版社

Springer

Tingyun Kuang
Congming Lu
Lixin Zhang

Photosynthesis Research for Food, Fuel and the Future

15th International Conference on Photosynthesis

Tingyun Kuang
Congming Lu
Lixin Zhang

Photosynthesis Research for Food, Fuel and the Future

15th International Conference on Photosynthesis

With 508 figures

ZHEJIANG UNIVERSITY PRESS
浙江大学出版社

Springer

Editors:
Prof. Tingyun Kuang
key Laboratory of Photobiology
Institute of Botany
Chinese Academy of Sciences
Beijing, China
Email: kuangty@ibcas.ac.cn

Prof. Congming Lu
Head, Photosynthesis Research Center
Institute of Botany
Chinese Academy of Sciences
Beijing, China
Email: lucm@ibcas.ac.cn

Prof. Lixin Zhang
key Laboratory of Photobiology
Institute of Botany
Chinese Academy of Sciences
Beijing, China
Email: zhanglixin@ibcas.ac.cn

ISBN 978-7-308-09694-2
Zhejiang University Press, Hangzhou

ISBN 978-3-642-32033-0
Springer Heidelberg New York Dordrecht London

ISBN 978-3-642-32034-7 (eBook)

Library of Congress Control Number: 2012943604

Preface

Photosynthesis is a natural process that converts solar energy to chemical energy. It is widely distributed in many different organisms, ranging from plants to bacteria. It provides all the food we eat and all the fossil fuel we use. Photosynthesis has long been studied in order to understand its underlying mechanisms and then to apply this knowledge to produce energy and food for the needs of our society.

The 15th international conference on photosynthesis was successfully held on 22–27 August 2010, in Beijing, China. The conference was organized by the Institute of Botany, Chinese Academy of Sciences and International Society of Photosynthesis Research. The conference had a fantastic scientific program and featured eminent speakers and state-of-the-art symposium speakers who are at the cutting edge of discovery in their field. These speakers provided an exciting scientific program which covered the breadth and depth of photosynthesis from molecular to global.

Under the conference theme, "photosynthesis research for food, fuel and the future", a total of 24 chapters were collected in this proceeding which contained twenty-three sections, each section representing one of the topics covered by plenary lectures and sessions at the conference. Therefore, the papers contained in this proceeding include all aspects of photosynthesis. We thank all conference participants and in particular those whose chapters are published here.

It is our belief that the Proceeding of the 15th International Conference on Photosynthesis will provide an opportunity for students, postdoctoral fellows and scientists from all over the world to enjoy the latest advanced developments on photosynthesis.

Tingyun Kuang
Chairman of Organizing Committee of
15th International Conference on
Photosynthesis, 2010, Beijing
10 January 2012

Contents

Symposium 01　Type I Reaction Centres

Symposium 02　Type II Reaction Centres

Symposium 03 Light Harvesting Anaerobic Systems

Symposium 04 Light Harvesting Aerobic Systems

Symposium 05 Bioenergetics of Photosynthetic Electron Flow

Symposium 06 Mechanisms of Water Oxidation

Symposium 07 Mimicking Photosynthetic Catalysis

Symposium 08 Regulation of Electron Transfer

Symposium 9 Control of the Calvin-Benson Cycle

Symposium 10 CO_2 Concentrating Mechanisms

Symposium 11 C_3, C_4 and CAM and Genetic Engineering

Symposium 12 Regulation of Photosynthetic Gene Expression

Symposium 13 Computational Systems Biology

Symposium 14 Biogenesis of Photosynthetic Apparatus

Symposium 15 Assembly of Photosynthetic Protein Complexes

Symposium 16 Photoprotection, Photoinhibition and Dynamics

Symposium 17 Perception of Environmental Stress and Acclimation

Symposium 18 Organelle Communication

Symposium 19 Marine Photosynthesis and Global Impact

Symposium 20 Crop Yield Improvement

Symposium 21 Microbial Derived Biofuels

Symposium 22 Photosynthesis and New Environmental Challenges

Symposium 23 Global Photosynthesis and Climate Change

Symposium 24 Photosynthesis Education

Symposium 01

Type I Reaction Centres

Deconvolution Analysis of Photoacoustic Waves of Electron Transfer in Photosystem I of *menG* Null Mutant of *Synechocystis* sp. PCC 6803

Xuejing Hou[a], Lien-Yang Chou[a], Harvey JM Hou[a,*]

[a]Department of Chemistry and Biochemistry, University of Massachusetts Dartmouth, North Dartmouth, massachusetts 02747, USA.
[*]Corresponding author. Tel. No. +01 508 999 8234; Fax No. +01 508 999 9167; E-mail: hhou@umassd.edu.

Abstract: Inactivating the *menG* gene causes 2-phytyl-1,4-naphthoquinone (Q) to be presented as a quinone acceptor in PSI of *Synechocystis* sp. PCC 6803. The electron transfer from Q^- to F_X is slowed to 600 ns in the *menG* null mutant [Sakuragi Y, B Zybailov G Shen, AD Jones, PR Chitnis, A van der Est, R Bittl, S Zech, D Stehlik, JH Golbeck, and DA Bryant. (2002) *Biochemistry* 41: 394-405]. Despite of the alternation of kinetics, the thermodynamics of electron transfer in the mutant is not known. In this work, we conducted deconvolution analysis on photoacoustic waves of the menG null mutants and the wild type strains of *Synechocystis* sp. PCC 6803 obtained by pulsed photoacoustics on the microsceond time scale. The fit by convolution of *menG* photoacoustic waves revealed a large volume contraction (-28 ± 2 Å^3) for the $P_{700}^* \rightarrow Q$ step and a positive volume change ($+5 \pm 2$ Å^3) for the $Q^- \rightarrow F_{A/B}$ step. The enthalpy changes were -0.7 ± 0.2 eV for the $P_{700}^* \rightarrow Q$ step and $+0.5 \pm 0.2$ eV for the $Q^- \rightarrow F_{A/B}$ step, respectively. Taking the free energy of –0.7 eV and –0.1 eV for these steps, the data presented here shows that the Q^- to $F_{A/B}$ electron transfer step in the *menG* null mutant is entropy driven.

Keywords: Enthalpy; Entropy; Volume change; Photoacoustics; Electron transfer; Photosystem I; *menG*

Introduction

Photosynthesis involves a series of light driven electron transfer steps in the reaction center to store the solar energy into the electrochemical energy. Photoacoustic method has been applied to gain new insights into enthalpy and volume changes associated with light driven reactions in photosynthesis (Delosme *et al*., 1994; Hou *et al*., 2001a; Hou *et al*., 2001b; Losi *et al*., 2003).

Application of photoacoustic signal deconvolution procedures is able to resolve the thermodynamic parameters of elemental steps (Small *et al*., 1992). The photoacoustic signal is the convolution between instrument response function and a time-dependent pressure evolution. The photoacoustic reference delivers all the absorbed energy into the medium as prompt heat. The singal of photoacoustic reference is thus the signal of the instrument response. After convolution, ther resulting simulated signal is compared to the measure photoascoustic waves of photoactive sample. The fit by convolution of photoacoustic waves on the nanosecond and microsecond time scales resolves two kinetic components in photosystem I from *Synechocystis* 6803 (Hou and Mauzerall, 2006).

Inactivating the *menG* gene causes 2-phytyl-1,4-naphthoquinone (Q) to be presented as a quinone acceptor in PSI of *Synechocystis* sp. PCC 6803. The electron transfer from Q^- to F_X is slowed to 600 ns in the *menG* null mutant (Sakuragi *et al*., 2002). Despite of the alternation of kinetics, the thermodynamics of electron transfer in the mutant is not known. In this work, we conducted deconvolution analysis on photoacoustic waves of the *menG* null mutants and the wild type strains of *Synechocystis* sp. PCC 6803 obtained by pulsed photoacoustics on the microsecond time scale.

Materials and Methods

Preparation of Purified PS I Trimers

PS I trimers were isolated from *Synechocystis* sp.

PCC 6803 and purified according to published methods (Sakuragi *et al*., 2002). For photoacoustic measurements, the sample buffer was replaced by ultrafiltration over a Centriprep YM-50 membrane with pH 8.0, 10 mmol N-[2-hydroxyethyl] piperazine-N'-2-ethanesulfonic acid (HEPES), and 0.03% dodecyl-R-D-maltoside (DM) without sucrose or glycerol.

Photoacoustic Measurements

The pulsed time resolved photoacoustic setup on the microsecond time scale. The light beam was produced by a Nd:YAG laser (Surelite) and an optical parametric oscillator (OPO, Surelite). An excitation wavelength of 680 nm was selected to excite the PS I centers.

Deconvolution Analysis of Photoacoustic Waves

The methodology and procedures of deconvolution of photoacoustics were similar to those described previously (Feitelson and Mauzerall, 2002; Hou and Mauzerall, 2006; Small *et al*., 1992). A deconvolution procedures of photoacoustic waves uses a commercial software Sound Analysis (Version 1.50 D) from Quantum Northwest, Inc. Assuming the photoacoustic wave represents a convolution between the photoacoustic reference and a sum of exponents (Small *et al*., 1992).

$$S(t) = R(t) * \sum_i \frac{\alpha_i}{\tau_i} e^{-\frac{t}{\tau_i}} \quad (1)$$

Where *R(t)* and *S(t)* are the photoacoustic reference and sample waves; α_i and τ_i are the photoacoustic intensity factor and deay lifetime for the ith component in the sum of exponentials. The asterisk (*) represents the convolution process. The analysis assumes that the noise on the photoacoustic waves is Gaussian.

Results and Discussion

Photoacoustics provides directly the volume and enthalpy change of photochemical reaction using calorimetry. We have previously reported the thermodynamic parameters of electron transfer in menA and menB null nutant PSI from *Synechocystis* sp. PCC 6803 on the microsecond time scale (Hou *et al*., 2009). However, our convolution analysis on *menA/B* PS I failed to resolve any convincing parameter for the plastoquinone anion to $F_{A/B}$ step. One main reason may be due to its long lifetime of 15 – 300 μs. In the *menG* null mutant, the electron transfer from Q^- to F_X is 600 ns (Sakuragi *et al*., 2002). The 600 ns time constant in *menG* null PS I is within the 1-μs time window and makes the extraction of its thermodynamic parameters possible.

Fig. 1 showed a typical fit by convolution of *menG* photoacoustic signal. The best simulation fit gave a prompt component less than 10 ns and a slow component with a lifetime of 600 ns. The prompt component is attributed to the charge separation to produce $P_{700}^+Q^-$; and the 600 ns component is attributed to the subsequent electron transfer from Q^- to $F_{A/B}$ step.

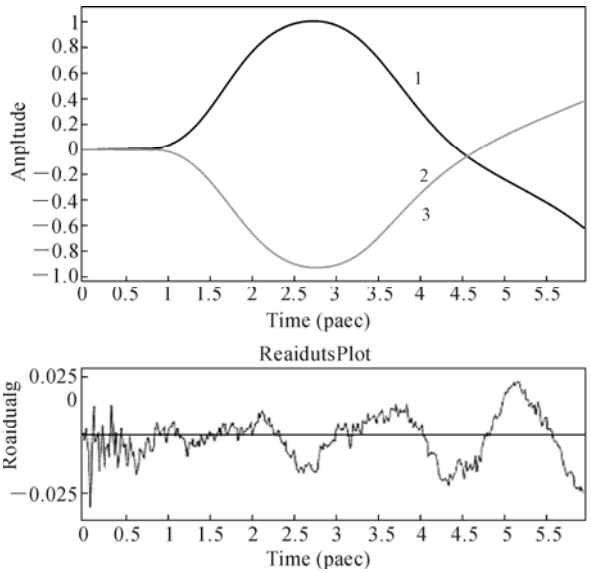

Fig. 1 Deconvolution of photoacoustic waves of PSI complexes from *menG* null mutant of *Synechocystis* sp. PCC 6803 at 25 °C. Upper panel: Curve 1 is the photoacoustic wave of the reference ink. Curve 2 is the photoacoustic signal of the *menG* null PS I complexes. Curve 3 is the simulation fit using convolution equation and gives prompt amplitude of –1.01 and a 600 ns component with amplitude of 0.19. Lower panel: The residue signal of the convolution fit.

The volume and enthalpy changes of electron transfer steps in *menG* null mutant can be obtained by plotting the amplitudes of deconvolution analysis multiplying the compressibility of water versus expansivity of water. The detailed description of photoacoustic data analysis to retrieve the thermodynamic parameters was reported previously (Hou *et al*., 2001b). As in Fig. 2, the charge separation and subsequent electron transfer in wild type photosystem I offer a large volume contraction and negative enthalpy change for the first step and a small volume contraction and positive enthalpy change for the second step. Similarly, the *menG* null mutant gave negative enthalpy change first and followed by a positive enthalpy change. In contrast, the volume change in the *menG* null mutant for the Q^- to $F_{A/B}$ step was a volume expansion and not volume contraction.

Table 1 Molecular volume change, enthalpy, free energy, and entropy change of electron transfer in PS I from the *menA/B null (Hou et al*., 2009*)*, *menG* null and wild type strains of *Synechocystis* sp. PCC 6803 (Hou and Mauzerall, 2006).

	ΔV, Å^3	ΔH, eV	ΔG, eV	–TΔS, eV
WT PSI (Hou *et al.*, 2006)				
$P_{700}^* \rightarrow A_1$	–21	–0.8	–0.7	+0.2
$A_1^- \rightarrow F_{A/B}$	–3	+0.4	–0.1	–0.5
*men*A/B PSI (Hou *et al*., 2009)				
$P_{700}^* \rightarrow A_P$	–17	–0.7	–0.7	0
$A_P^- \rightarrow F_{A/B}$	–9	+0.3	–0.1	–0.4
menG PSI (This work)				
$P_{700}^* \rightarrow Q$	–28	–0.7	–0.7	0
$Q^- \rightarrow F_{A/B}$	+5	+0.5	–0.1	–0.5

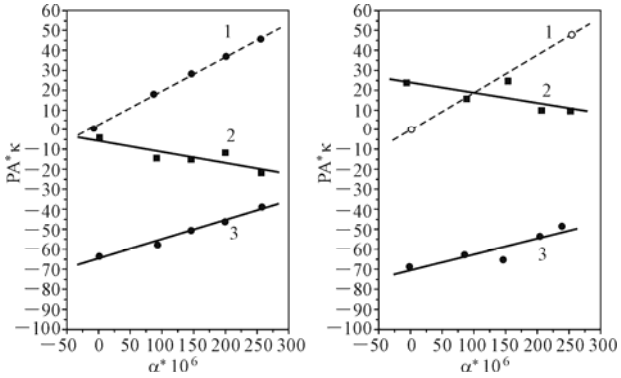

Fig. 2 Plots of amplitude times compressibility versus expansivity of the wild type PSI redraw from the ref (Hou and Mauzerall, 2006) with permission from the American Chemical Society and *menG* null PSI of *Synechocystis* sp. PCC 6803. Left panel: Curve 1 is the reference. Curve 2 is the 100 ns component. Curve 3 is the prompt component. Right panel: curve 1 is a photoacoustic reference signal. Curve 2 is the 600 ns component. Curve 3 is the prompt component. The enthalpies and volume changes are listed in Table 1.

Table 1 lists the thermodynamic parameters of charge separation and subsequent electron transfer in *menA/B*, *menG*, and wild type photosystem I of *Synechocystis* 6803. The *menG* null mutant revealed a large volume contraction (−28 ± 2 Å^3) for the $P_{700}^* \rightarrow$ Q step and a positive volume change (+5 ± 2 Å^3) for the $Q^- \rightarrow F_{A/B}$ step. These numbers are different from those in menA/B (–17 Å^3 and –9 Å^3) and wild type photosystem I (–21 Å^3 and –3 Å^3). This is largely due to the difference in the chemical structure of the quinone acceptors: A_1 (2-methyl-3-phytyl-1,4-naphthoquinone) in wild type, A_P (plastoquinone-9) in *menA/B*, and Q (2-phytyl-1,4-naphthoquinone) in *menG* photosystem I. As the quinone-binding pocket is naturally designed for the A_1, the foreign quinones (A_P and Q) would cause changes in the binding moiety of protein including compressibility and polarity of protein.

The volume contraction caused by electrostriction can be expressed using the equation:

$$\Delta V_{el} = \frac{\partial \Delta G_{el}}{\partial P} = \left(\frac{e^2 \cdot \kappa}{2 \cdot \varepsilon}\right) \times \left(\frac{\partial \ln \varepsilon}{\partial \ln V}\right) \times \left[\frac{z_+^2}{r_+} + \frac{z_-^2}{r_-} + \frac{2 z_+ z_-}{r_\pm}\right] \quad (2)$$

where ΔV_{el} is electrostriction, ΔG_{el} is the Born charging energy, P is pressure, z^+, z^- are the signed charge on the positive and negative ions, κ is compressibility of the protein, V its molar volume, ε its dielectric coefficient, r_+ and r_- the radii of the donor and acceptor (assumed previously neutral) and $r\pm$ is the distance between the two ions.

The large tail in plastoquinone (AP) may decrease the compressibility of protein. Additionally, the small size of plastoquinone may allow a water molecule to present in the pocket and increase the polarity of protein and effective dielectric coefficient (ε). These decease the volume change (ΔV_{el}). In the case of *menG* null mutant, the Q lacks the 2-methyl group and thus creates a looser and more polar quinone pocket. Similar effect of small size quinones on volume changes was reported previously in bacterial reaction centers with different quinones (Edens *et al*., 2000).

The enthalpy changes of charge separation and electron transfer in *menG* null mutant were –0.7 ± 0.2 eV for the $P_{700}^* \rightarrow$ Q step and +0.5 ± 0.2 eV for the $Q^- \rightarrow F_{A/B}$ step, respectively. Taking the free energy of –0.7 eV and –0.1 eV for these steps, the data presented here indicates a key role of the apparent entropy in the Q^- to $F_{A/B}$ electron transfer step in the *menG* null mutant.

In the *menA/B* null mutant, deconvolution analysis

failed to resolve the 15 μs component (Hou *et al*., 2009). Assume the overall reaction in *menA/B* photosystem I is similar to that of wild type photosystem I, we infer the electron transfer from A_P^- to $F_{A/B}$ step is entropy driven. In this work, we resolve the 600 ns component and demonstrated the Q^- to $F_{A/B}$ step is entropy driven. In addition, the entropy driven reaction for A_1^- to $F_{A/B}$ step in wild type photosystem I was reported. We concluded that the entropy driven reaction in *Synechocystis* photosystem I is not affect by recruitment of foreign quinone. The observation of entropy driven reaction in photosystem is explained as vibrational effect which is due to the loosening of protein structure and decrement of interaction in protein (Hou and Mauzerall, 2006). Recently, the significant entropy change was observed for charge separation in artificial photosynthesis (Rizzi *et al*., 2008). We believe that the driving force of electron trasfer is not only dependent on the bonding energy of cofactors (enthalpy) but also on the available states of interaction of proteins (entropy).

Acknowledgements

We thank Prof. Mauzerall for his continuous support. The photoacoustic measurements were conducted in Prof. Mauzerall laboratory. We thank Prof. Golbeck and Dr. Gaozhong Shen for providing the *menG* null samples. We also thank Fan Zhang for assistance in data analysis and Wanshu He for helpful discussions. This work is supported by the University of Massachusetts Dartmouth.

References

Delosme R, D Beal, P Joliot (1994) Photoacoustic Detection of Flash-Induced Charge Separation in Photosynthetic Systems. Spectral Dependence of the Quantum Yield. Biochim. Biophys. Acta. 1185: 56-64

Edens GJ, MR Gunner, Q Xu, D Mauzerall (2000). The Enthalpy and Entropy of Reaction for Formation of $P^+Q_A^-$ from Excited Reaction Centers of Rhodobacter Sphaeroides. J. Am. Chem. Soc. 122: 1479-1485

Feitelson JD Mauzerall (2002) Enthalpy and Electrostriction in the Electron-Transfer Reaction between Triplet Zinc Uroporphyrin and Ferricyanide. J. Phys. Chem. B. 106: 9674-9678

Hou HJM, D Mauzerall (2006) The A-FX to FA/B Step in Synechocystis 6803 Photosystem I is Entropy Driven. J. Am. Chem. Soc. 128: 1580-1586

Hou HJM, G Shen, VA Boichenko, JH Golbeck, D Mauzerall (2009) Thermodynamics of Charge Separation of Photosystem I in the MenA and MenB Null Mutants of Synechocystis sp. PCC 6803 Determined by Pulsed Photoacoustics. Biochemistry 48: 1829-1837

Hou JM, VA Boichenko, BA Diner, D Mauzerall (2001a) Volume Change, Enthalpy, and Entropy of Electron Transfer Reactions in Manganese-Depleted Photosystem II Core Complexes. Biochemistry 40: 7117-7125

Hou JM, VA Boichenko, YC Wang, PR Chitnis, D Mauzerall (2001b) A Pulsed Photoacoustic Study of Electron Transfer in Photosystem I Reveals a Similarity to Bacterial Reaction Centers in Both Volume Change and Entropy. Biochemistry 40: 7109-7116

Losi A, I Yruela, M Reus, AR Holzwarth, SE Braslavsky (2003) Structural Changes upon Excitation of D1-D2-Cyt b559 Photosystem II Reaction Centers Depend on the β-carotene Content. Photochem. Photobiol. Sci. 2: 722-729

Rizzi AC, M van Gastel, PA Liddell, RE Palacios, GF Moore, G Kodis, AL Moore, TA Moore, D Gust, SE Braslavsky (2008) Entropic Changes Control the Charge Separation Process in Triads Mimicking Photosynthetic Charge Separation. J. Phys. Chem. A. 112: 4215-4223

Sakuragi Y, B Zybailov, G Shen, AD Jones, PR Chitnis, A van der Est, R Bittl, S Zech, D Stehlik, JH Golbeck, DA Bryant (2002) Insertional Inactivation of the MenG Gene, Encoding 2-phytyl-1,4-naphthoquinone Methyltransferase of Synechocystis sp. PCC 6803, Results in the Incorporation of 2-phytyl-1,4-naphthoquinone into the A_1 Site and Alteration of the Equilibrium Constant between A_1 and F_X in Photosystem I. Biochemistry 41: 394-405

Small JR, LJ Libertini, EW Small (1992) Analysis of Photoacoustic Waveforms Using the Nonlinear Least Squares Method. Biophys. Chem. 42: 29-48

Towards Uncovering the Energetics of Secondary Electron Transfer Reactions in Photosystem I

Stefano Santabarbara[a,b*], Fabrice Rappaport[c], Kevin Redding[a]

[a]Department of Chemistry and Biochemistry, Arizona State University, Tempe, U.S.A.;
[b]Institute de Biologie Physico-Chimique, Paris, France;
[C]Instituto di Biofisica, Consiglio Nazionale delle Ricerche, Milano, Italy.
[*]Corresponding author. Tel. No. +39 2 503 14857; Fax No. +39 2 503 14815; E-mail: stefano.santabarbara@cnr.it.

Abstract: Phylloquinone (PhQ) acts as the secondary electron acceptor in the reaction centre of Photosystem I. At room temperature the semiquinone anion is oxidized with complex multiphasic kinetics by electron transfer to the iron-sulphur cluster F_X. The two principle phases of the oxidation kinetics are characterized by lifetimes of 20 ns and 250 ns. The 20-ns phase is associated primarily with the oxidation of PhQ_B, which is bound by the PsaB subunit, and the 250-ns phase is associated with oxidation of PhQ_A, which is bound by the PsaA subunit. The difference of about one order of magnitude between the two oxidation lifetimes can be explained by considering the difference in the driving force for oxidation of the PhQ_A ($\Delta G^0 > 0$) and PhQ_B ($\Delta G^0 < 0$) semiquinone forms. Such an energetic scenario also promotes a transient electron transfer from PhQ_A^- to PhQ_B, with F_X acting as an intermediary.

Keywords: Photosystem I (PS I); Electron Transfer (ET); Reaction centre (RC); Phylloquinone; Iron-sulphur clusters

Introduction

Photosystem I (PS I) is a large macromolecular chromophore-protein supercomplex serving as a fundamental component of the oxygenic photosynthesis. The core of PS I, which is well conserved in different organisms, harbours all the cofactors involved in light-induced electron transfer (ET) as well as about ~100 Chlorophyll (Chl) *a* and 30 β-carotene molecules, acting as the internal antenna. Crystallographic models have been solved for core complexes from cyanobacteria (Jordan *et al*., 2001) and core-light harvesting supercomplexes of higher plants (Ben-Shem *et al*., 2003). Both structures shows a symmetric arrangement of the cofactors involved in ET reactions, which are organized in two chains, each of which is coordinated primarily by either the PsaA or by the PsaB subunit of the reaction centre (RC), with the exception of the terminal electron acceptors, the iron-sulphur clusters F_A and F_B, which are bound to PsaC. Symmetric arrangement of ET cofactors is a common structural feature in photosynthetic RCs, and is also observed also in the structural models of Type II RCs (PS II and purple bacteria RCs). However, whereas in Type II RCs only one of the two chains is active in ET reactions (*i.e.*, asymmetric or unidirectional ET), there is a general consensus that both ET chains are functional in PS I, which operates according to a so-called bidirectional ET mechanism (Santabarbara *et al*., 2005a; Rappaport *et al*., 2006; Srinivasan and Golbeck, 2009). The functionality of both ET branches has been observed primarily by monitoring the effect of site-directed mutations of cofactor bound by primarily either by PsaA (ETC_A chain) or PsaB (ETC_B chain) on the kinetics of oxidation of the secondary electron acceptor, Phylloquinone (PhQ). At room temperature the oxidation of semiquinone form (PhQ^-) is described by a minimum of two exponential functions characterised by lifetimes of 15–25 ns and 200–300 ns (depending on the organism and preparation) (Santabarbara *et al*., 2005a; Rappaport *et al*., 2006). It was shown that mutations affecting the binding of PsaA-bound

phylloquinone (PhQ_A) altered the lifetime of the 250-ns phase only, whereas mutation of PhQ_B (PsaB-bound) affected the 20-ns lifetime only. At the same time, the amplitude of these phases, which in WT is ~1:2 (20-ns:250-ns) is not affected by the mutations (Guergova-Kuras *et al*., 2001; Byrdin *et al*., 2006). Altering the binding of the primary electron donor, Chl A_0, the cofactors located upstream to the PhQs, affected the amplitude (redistribution) without significant modification of the lifetimes (Li *et al*., 2006; Byrdin *et al*., 2006). More recently, the effect of mutating the A_0 binding site, on both subunits, was also monitored directly on the kinetics of primary charge separation (Müller *et al*., 2010). To a good approximation, it is also possible to assign, the 20-ns phase to PhQ_B^- oxidation and the 250-ns PhQ_A^- oxidation, whereas the amplitude of the two phases are determined at the level of primary charge separation. Still, the reason for the ~10-fold difference in PhQ_A^- and PhQ_B^- oxidation lifetimes remains unclear. Structurally the two PhQs are substantially equi-distant from the electron acceptor F_X, which is shared by both ET chains. Thus, it is likely that differences in lifetimes arises from different physical-chemical properties of PhQ_A and PhQ_B induced by the interaction with the respective protein host. The structures suggest two principal interactions PhQ-subunit interactions: (i) π-stacking between the naphthyl ring of PhQ and the indole of a nearby Trp residues, and (ii) asymmetric H-bonding to the C2-keto group of PhQ from the backbone amide of a specific Leu residue (PsaA-L722; PsaB-L708). Whereas the effect of mutating the conserved tryptophans (and other amino acids affecting the hydrophobicity of the binding site) have been already investigated, the impact of H-bonding on the energetics is less studied, also because it virtually impossible to suppress the bond. Here we discuss the effect of substituting the natural Leu residues with Threonine and Tyrosine, both of which possess larger side chain, hence potentially perturbing the interaction indirectly through steric hindrance effects. We also present a discussion of the effect of point mutations affecting PhQ binding, and their effect in controlling the redox properties of these cofactors.

Materials and Methods

Construction of point mutations of PsaA and PsaB subunits of PS I in *C. reinhardtii* was performed as described (Byrdin *et al*., 2006). For spectroscopic investigations, mutations were engineered in the P71-Fud7 genetic background, a strain lacking PS II and most of the external antenna complement. As the P71-Fud7 harbours a wild-type PS I, we refer hereafter to this strain simply as WT.

The kinetics of secondary ET in PS I was studied by time-resolved absorption difference spectroscopy, using a pump-probe set-up previously described in detail (Beal *et al*., 1999). In brief, actinic excitation (pump) is from a dye (LDS 698) laser pumped by a frequency-doubled ND-YAG laser. The excitation pulse is centred at 700 nm, has a duration of ~5 ns, and is attenuated to excite about 70% of the reaction centres. The measuring (probe) pulse is from the output of a tuneable OPO, pumped by a frequency-tripled Nd-Yag laser. For measurements in the UV, the output of the OPO is frequency doubled. The pump-probe delay is controlled by a home-built pulse programmer. The resolution of the instrumentation is ~ 5 ns, without deconvolution of the actinic pulse. The kinetics, acquired at several different wavelengths, are fitted globally to a sum of exponentials, yielding lifetimes (τ) and their decay associated spectra (DAS). Fitting is obtained by a non-linear least square Levernberg-Marquart algorithm that minimises χ^2.

Results

Fig. 1 shows the kinetics of transient absorption in the 10 ns to 20 μs time window, monitored at 390 nm, which is close to the maximal differential absorption difference of the PhQ^--PhQ spectrum, recorded in whole cells of the WT and two mutants of *C. reinhardtii* in which the π-stacking residue on the PsaA subunit (W697, numbering is that of *Synechococcus elongatus*) has been substituted with a phenylalanine (W697F, Fig. 1B) and leucine (W697L, Fig. 1C). Global fitting of the kinetics (not shown) yields three exponential lifetimes in all cases, plus a non-decaying component. The relative contributions of each lifetime to the total absorption transient are also shown in Figs. 1A, 1B and 1C. The slowest of these decay lifetimes (~6 μs) is assigned to the reduction of P_{700}^+ based on its DAS. As observed in previous studies, the value of this lifetime and its associated spectrum are not affected by mutations of PhQ binding site (*i.e.*, Rappaport *et al*., 2006). Hence, it will not be discussed further. The two remaining

lifetimes fall in the nanosecond regime, as also previously reported (reviewed in Rappaport *et al*., 2006) and are characterised by values of 24 and 256 ns: these lifetimes are assigned to PhQ^- oxidation.

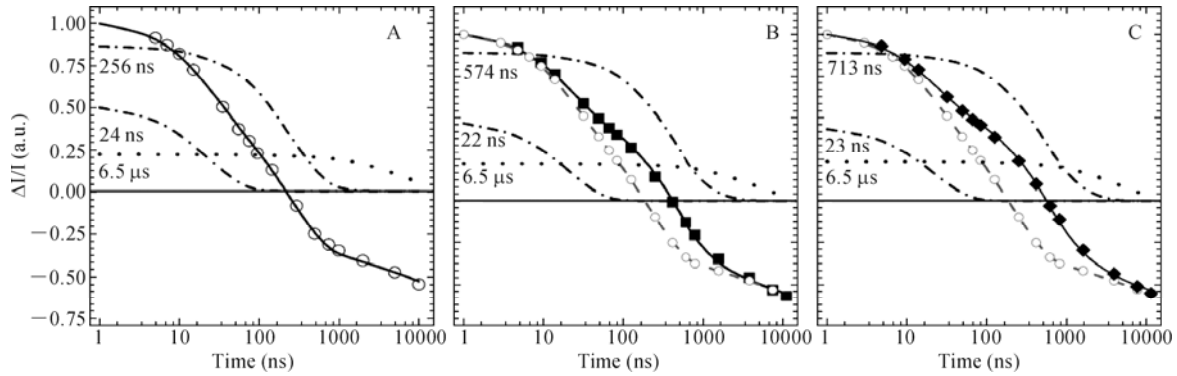

Fig. 1 Kinetics of ET monitored at 390 nm in WT (A) PsaA-W697F (B), and PsaA-W697L (C) mutants. Experimental: solid symbols: mutant, open symbols: WT. Solid line: fit to the kinetics. Dashed-dot line: contribution of "fast and slow" phase of PhQ^- oxidation, dotted line: P_{700}^+ reduction.

As commonly observed, in all three strains, the fastest lifetime is in the range of 22–24 ns; the differences fall in the margin of errors. In contrast, the slowest phase of PhQ^- oxidation is slowed to 574 ns in PsaA-W697F and 713 ns in PsaA-W697L.

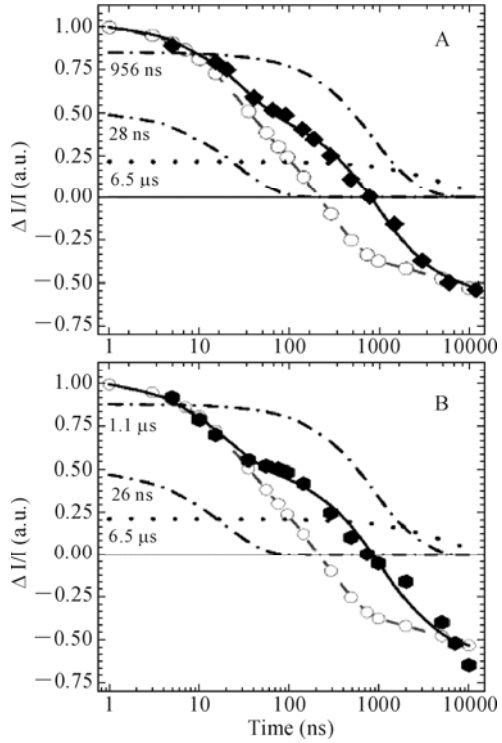

Fig. 2 Kinetics of ET monitored at 390 nm in PsaA-S692A (A) and PsaA-F689W (B) mutants. Line and symbols as in Fig.1.

Fig. 2 shows the kinetics of ET, also monitored at 390 nm, in mutants of two conserved residues, PsaA-S692A and PsaA-F689W. The latter residue contributes to the hydrophobic environment. As observed in the other PhQ_A site mutants, the lifetime of the 25 ns component is unchanged in the PsaA-S692A and PsaA-F689W mutants, whereas that of 250-ns phase is significantly slower, characterized by values of 956 ns (PsaA-S692A) and 1089 ns (PsaA-F689W). Another crucial feature is that in all these mutants, as well as in others already investigated but not presented here (*e.g.* Rappaport *et al.*, 2006), the relative amplitude of the 20 ns to 250 ns is not affected by the mutations; within the confidence interval it remains about 1:2, as measured by the PhQ difference absorption in the near UV.

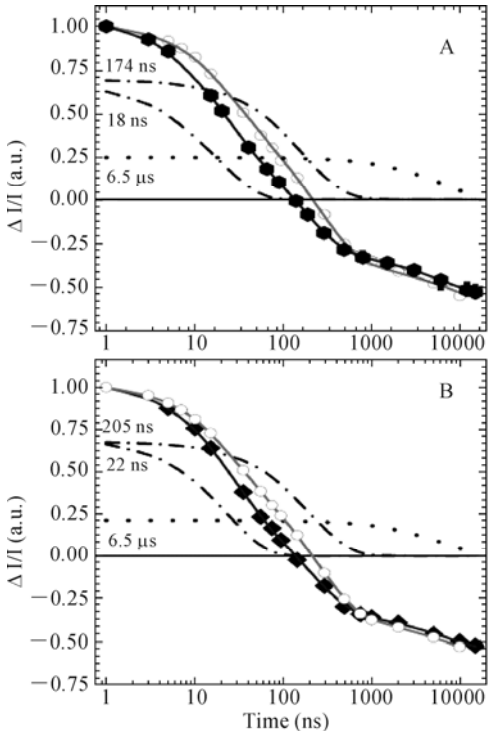

Fig. 3 Kinetics of ET monitored at 390 nm in PsaA-L722T (A) and PsaA-L722Y (B) mutants. Line and symbols as in Fig. 1.

Fig. 3 shows the kinetics of PhQ^- oxidation in two mutants designed to perturb the H-bonding between the protein backbone and the naphthoquinone moiety, by exchanging the conserved residue PsaA-L722, with a tyrosine and threonine (PsaA-L722Y/T). Both mutations designed to perturb H-bonding have little effect on the value of the fast PhQ^- oxidation phase (Fig. 3). Interestingly, both in PsaA-L722Y (205 ns) and PsaA-L722T (174 ns), the lifetime characterizing the slowest PhQ^- oxidation phase becomes faster than in WT (248 ns), whereas other mutations had the opposite kinetic effect (*i.e.* Figs. 1 and 2). Moreover, again in contrast to observation in other mutations of conserved residues, we observe a redistribution of the fast:slow phases of PhQ^- oxidation from 1:2 in WT to ~1:1 in PsaA-L722Y/T (Fig. 3). This redistribution of the amplitudes is observed not only at 390 nm, but throughout the most characteristic spectral features of the DAS (data not shown, but see Santabarbara *et al*., 2010a).

Hence, whereas these mutants provide further confirmation for the bidirectional model, as mutants of PsaA subunit affect essentially only the lifetime of the slowest phase of PhQ^- oxidation, which is therefore assignable primarily to PhQ_A^- kinetics, some peculiar effect of these mutation, such as acceleration of the kinetics and, especially, apparent redistribution of the amplitude of the oxidation phases require reconsidering the details of secondary ET kinetics in PS I.

Discussion

We have then sought a plausible explanation capable of accommodating observations gathered on all mutants affecting π-stacking interactions and H-bonding to PhQ, by implementing a kinetic model describing secondary ET reactions in PS I (Fig. 4). In this model we consider only the ET reactions, involving PhQ_A, PhQ_B and F_X, and the kinetics are obtained by the solution of a system of linear differential equations. The rate of electron transfer between couples of acceptors-donor cofactors can be described according to tunnelling formalism as:

$$k_{ET} = \frac{2\pi}{\hbar}\frac{|H_{DA}|^2}{\sqrt{4\pi\lambda_{tot}\mathrm{k}_b\mathrm{T}}}\exp\left[-\frac{(\lambda_{tot}+\Delta G^0)^2}{4\lambda_{tot}\mathrm{k}_b\mathrm{T}}\right] \qquad (1)$$

where $|H_{DA}|$ is the electronic element of the Hamiltonian, λ_{tot} is the total reorganization energy, ΔG^0 is the standard Gibbs free energy difference, and all the other terms have their usual physical meaning.

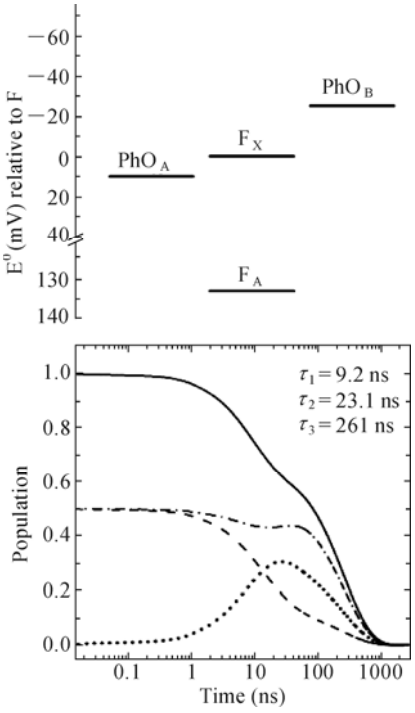

Fig. 4 Simulation of ET kinetics in WT PS I. Top: energetic scheme. Bottom: calculated population evolution of PhQ_B^- (dash), PhQ_A^- (dash-dot); F_X^{red} (dot). Total PhQ^- evolution, solid line.

To a good approximation, $|H_{DA}|$ depends exponentially on the donor-acceptor distance (r_{DA}), according to $|H_{DA}| = |H^0_{DA}|\exp[-\beta r_{DA}]$, where $|H^0_{DA}|$ is the is the value at contact and β is an attenuation factor, both of which are dependent on the tunnelling barrier. For ET in redox proteins it has been proposed that $|H^0_{DA}| = 4\times10^{-2}$ eV and β=0.7 $Å^{-1}$ (*e.g.* Moser *et al*., 1992). These values were used in our simulations. Moreover, it has been suggested that λ_{tot} displays a spread in redox-active protein, in the range of 0.6–1.0 eV. Hence, it is unlikely that there exist large differences in λ_{tot} for the reduction of F_X by $PhQ_{A/B}^-$ and we assumed that $\lambda_{tot} = 0.65$ eV for all the reactions considered; thus, only the values of ΔG^0 has to be tuned in order to simulate the experimental results. Finally, we consider $PhQ_A^-(0) = PhQ_B^-(0) = 0.5$, and $F_X^{red}(0) = 0$.

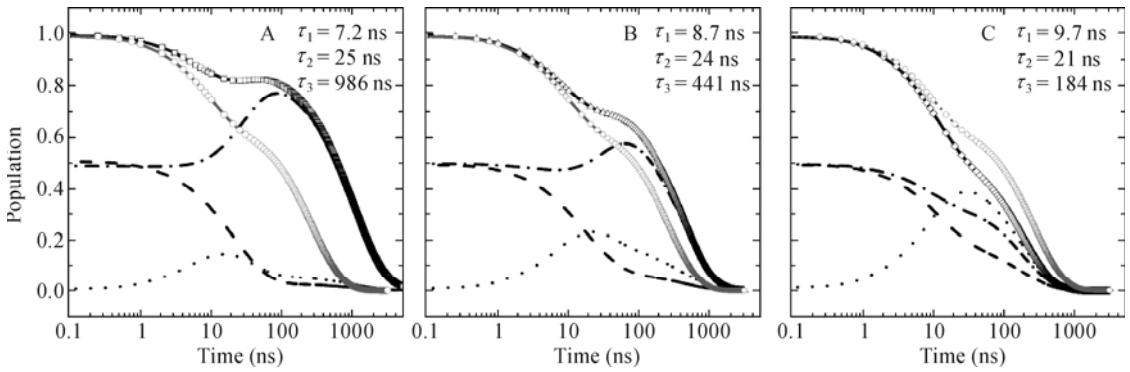

Fig. 5 Simulation of ET kinetics in PsaA-F689W (A), PsaA-W677F (B) and PsaA-L722T (C). Line and symbolds as in the legend of Fig. 4. Shown for comparison is the simulatuions in WT (grey lines and symbols).

The ET kinetics in the wild type can be satisfactorily simulated by assuming that $\Delta G^0_{PhQ_A \to F_X}$ = +10 meV and $\Delta G^0_{PhQ_B \to F_X}$ = –25 meV, *i.e.* the oxidation of PhQ_B^- is thermodynamically favourable and that of PhQ_A^- is unfavourable (Fig. 4). Similar suggestions have already been advanced and, as a corollary, they provide a simple explanation for the well-documented heterogeity of ET reactions at cryogenic temperatures (Santabarbara *et al*., 2005). It is worth noting that: (i) the kinetic model predicts three exponential lifetimes (as three stages are considered), and two of them are in the 5–30 ns interval, and describe the "fast" oxidation phase, while one is ~260 ns; (ii) the ratio of amplitudes of the fast:slow phases is 1:2, as in the experiments, starting from equal initial population of PhQ_A and PhQ_B; (iii) the calculated *rates* of PhQ_A (2.7×10^{-2} ns^{-1}) and PhQ_B (5.9×10^{-2} ns^{-1}) oxidation only differ by a factor of ~2, which is much less than the difference between lifetimes (~10).

Fig. 5 shows the simulations for the PsaA-W697F (A) and the PsaA-F695W (B) mutants. The effect of mutations affecting proximal and distal π-stacking, as well as change in hydrophobicity of the PhQ_A binding site, can be simulated satisfactorily by an increase $\Delta G^0_{PhQ_A \to F_X}$ of 25–60 meV, depending on the mutation (Fig. 6). Consistent with the experiments, the simulations predict a sizable effect only on the longer lifetimes, from 261 ns in ET to 441 (W697F) and 986 ns (F695W). We also predict a small redistribution of amplitudes (10%–15%) in favour of the slowest phase. This margin seems to exceed the experimental results. However, the predicted redistribution is relatively small, so that, considering the simplification employed in constructing the kinetic model, we consider this description overall satisfactorily.

In order to simulate H-bond (PsaA-L722 mutants) perturbation, (also shown in Fig. 5C), we need to decrease the value of $\Delta G^0_{PhQ_A \to F_X}$ by 10–20 meV (Fig. 6). This is consistent with a destabilization of semiquinone form of PhQ, making it a more reductive species, hence increasing the driving force for the reaction. Simulations of the PsaA-L718Y/T mutant's kinetics also predict a redistribution of (total) amplitudes for the fast and slow phases, which have almost identical amplitudes as observed in the experiments (Fig. 3). The macroscopic explanation for the observed amplitude redistribution is that the energetic configurations of WT, where PhQ_A represent a local thermodynamic minimum, favours transient electron transfer from PhQ_B to PhQ_A, via F_X in ns time scale. This transient electron transfer results in an enhancement of the total amplitude of 250 ns lifetime with respect to the initial population of PhQ_A (by A_{0A}^-). In the H-bond mutants, the driving force for $PhQ_B \to F_X \to PhQ_A$ transfer is dramatically reduced, so that the amplitude of this transfer process is decreased and the amplitude of fast and slow phases more closely resemble the initial populations (which were assumed identical). This type of kinetic modelling was extended to several other mutations, including those affecting PhQ_B binding, and a compilation of the estimated perturbations of $PhQ_{A/B}$ midpoint potential (determining ΔG^0) are presented in Fig. 6. It can be seen that, in all mutants examined so far, the perturbations ranges in $\pm 50 - 80$ mV. Whereas mutations that weaken the H-bond decrease the midpoint potential, those affecting hydrophobic interactions tend to increase its value. Surprisingly, the extent of the increase seems to be similar for residues that are located in proximity to the quinones (*e.g.* PsaA-W697/PsaB-W677) and residue that are more distal to them (*e.g.* PsaA-F689/PsaB-W673).

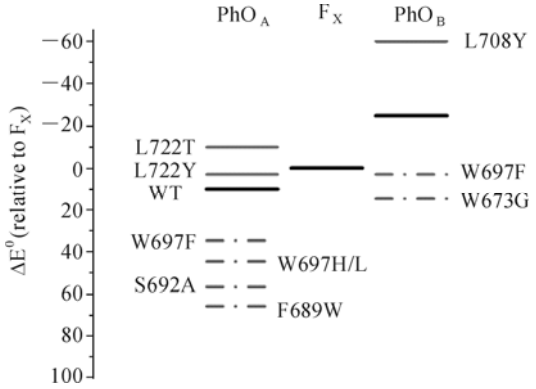

Fig. 6 Mutation-induced perturbation of redox potential of PhQ_A and PhQ_B derived from simulation of ET kinetics.

In conclusion, the difference in lifetimes describing PhQ oxidation in PS I RC can be rationalized assuming difference driving forces for PhQ_A and PhQ_B oxidation, with $\Delta G^0_{PhQ_A \to F_X} > 0$ and $\Delta G^0_{PhQ_B \to F_X} < 0$, respectively. This asymmetry in the energetic configurations of PhQ_A and PhQ_B promotes a transient inter-quinone electron transfer, mediated by F_X. Hydrophobic interactions play a central role in poising PhQ potential toward more reducing values, *i.e.* favouring rapid ET, whereas asymmetric H-bonding has the opposite effect. However, H-bonding might be required in order to stabilize the binding of quinone to the RC (Santabarbara *et al*., 2010).

Acknowledgements

Work in KR's laboratory was supported by Energy Biosciences grant DE-FG02-08ER15989 from the U.S. Dept. of Energy. FR acknowledges funding by CNRS and UPMC. SS thanks the CNR for funding.

References

Béal D, Rappaport F, Joliot P (1999) A New High-Sensitivity 10-ns Time-Resolution Spectrophotometric Technique Adapted to in Vivo Analysis of the Photosynthetic Apparatus. Rev. Sci. Instr. 70: 202-207

Ben-Shem A, Frolow F, Nelson N (2003) Crystal Structure of Plant Photosystem I. Nature 426: 630-635

Byrdin M, Santabarbara S, Gu F, Fairclough WV, Heathcote P, Redding K, Rappaport F (2006) Assignment of a Kinetic Component to Electron Transfer between Iron-Sulfur Clusters F_X and $F_{A/B}$ of Photosystem I. Biochim. Biophys. Acta. 1757: 1529-1538

Guergova-Kuras M, Boudreaux A, Joliot A, Joliot P, Redding K (2001) Evidence for two Active Branches for Electron Transfer in Photosystem I. Proc. Nat. Acad. USA 98: 4437-4442

Jordan P, Fromme P, Klukas O, Witt HT, Saenger W, Krauss N (2001) Three-dimensional Structure of Cyanobacterial Photosystem I at 2.5 Angstrom Resolution. Nature 411: 909-917

Li Y, van der Est A, Lucas MG, Ramesh VM, Gu F, Petrenko A, Lin S, Webber AN, Rappaport F, Redding K (2006) Directing Electron Transfer within Photosystem I by Breaking H-bonds in the Cofactor Branches. Proc. Natl. Acad. Sci. USA 103: 2144-2149

Moser CC, Keske JM, Warncke K, Farid RS, Dutton PL (1992) Nature of Biological Electron Transfer. Nature 355: 796-802

Müller MG, Slavov C, Luthra R, Redding KE, Holzwarth AR (2010) Independent Initiation of Primary Electron Transfer in the Two Branches of the Photosystem I Reaction Centre. Proc. Natl. Acad. Sci. USA 107: 4123-4128

Rappaport F, Diner BA, Redding K (2006) In Photosystem I: the Plastocyanin: Ferredoxin Oxidoreductase in Photosynthesis, Golbeck JH (ed.) Kluwer: Dordrecht, pp. 223-244

Santabarbara S, Heathcote P, Evans MCW (2005) Modelling of the Electron Transfer Reactions in Photosystem I by Electron Tunnelling Theory. Biochim. Biophys. Acta Bioenergetics 1708: 283-310

Santabarbara S, Reifschneider K, Jasaitis A, Gu F, Agostini G, Carbonera D, Rappaport F, Redding KE (2010a) Interquinone Electron Transfer in Photosystem I as Evidenced by Altering the Hydrogen Bond Strength to the Phylloquinone(s). J. Phys. Chem. B. 114: 9300-9312

Srinivasan N, Golbeck JH (2009) Protein-Cofactor Interactions in Bioenergetic Complexes: the Role of the A_{1A} and A_{1B} Phylloquinones in Photosystem I. Biochim. Biophys. Acta 1787: 1057-1088

Supercomplex Organizations and Evolution of Photosystems I and II (*Anabaena* sp. PCC 7120, *Cyanophora Paradoxa* and *Cyanidioschyzon Merolae*)

Mai Watanabe*, Hisako Kubota, Hajime Wada, Rei Narikawa, Masahiko Ikeuchi

Department of Life Sciences (Biology), Graduate School of Arts and Science, University of Tokyo, Komaba, Meguro, Japan.
*Corresponding author. Tel. No. +81 3 5454 4375; Fax No. +81 3 5454 4337; E-mail: MAIMAI@bio.c.u-tokyo.ac.jp.

Abstract: Supercomplex organization of photosystem complexes was studied in various cyanobacteria, a glaucocystophyte and a primitive rhodophyte by blue-native PAGE. As already shown in *Thermosynechococcus elongatus*, PSII complexes yielded the dimeric and monomeric forms. In any case, the recovery of the dimeric PSII was increased at high detergent concentrations. On the other hand, there were unexpected variations in the organization of the PSI supercomplexes depending on the species. In filamentous N_2-fixing cyanobacterium *Anabaena* sp. PCC 7120 and a glaucocystophyte *Cyanophora paradoxa* gave PSI tetramer and dimer but no trimer at all.

Keywords: *Anabaena*; Blue-native PAGE; *Cyanophora;* Photosystem; Supercomplex

Introduction

Functional photosystems I and II (PSI and PSII) have been isolated as a multisubunit membrane supercomplex from cyanobacteria, algae and land plants. It is known that the PSII complex functions as a dimer from cyanobacteria to land plants. On the other hand, it is generally accepted that the PSI complex functions as a trimer in cyanobacteria and as a monomer associated with light-harvesting chlorophyll complex (LHC) in algae and land plants. Crystal structures of the PSII dimer and PSI trimer from *Thermosynechococcus elongatus* and the PSI monomer from pea have been determined (Jordan *et al*., 2001; Ben-Shem *et al*., 2003; Guskov *et al*., 2009).

Previously, we reported the organization of PSII and PSI complexes of *T. elongatus* by blue-native PAGE (BN-PAGE) (Watanabe *et al*., 2009, 2011). The ratio of the PSII monomer to the dimer varied depending on the concentrations of with *n*-dodecyl-β-D-maltoside (DM). In contrast, the PSI complex was almost recovered as a trimer at wide concentrations of DM. Here we studied supercomplex organization of photosystems of various cyanobacteria, glaucocystophyte and primitive rhodophyte by BN-PAGE with wide range of detergent concentrations.

Materials and Methods

Thylakoid membranes of *Anabaena* sp. PCC 7120, *Synechocystis* sp. PCC 6803, *T. elongatus* and *Cyanidioschyzon merolae* 10D were isolated as described in Watanabe *et al*. (2009). Cyanelles from *Cyanophora paradoxa* strain NIES 547 were isolated as described in Koike *et al*. (2000). Isolated cyanelles were disrupted with zirconia beads as described in Watanabe *et al*. (2009). Thylakoid membranes [1 (mg Chl) ml^{-1}] were solubilized with DM on ice for 30 min, followed by centrifugation at 300,000 xg for 30 min at 4 ^{o}C. The solubilized supernatant was subjected to BN-PAGE and BN-PAGE gel was subjected to two-dimensional SDS-PAGE.

Results and Discussion

The thylakoid membranes from cyanobacteria, a glaucocystophyte and a primitive rhodophyte were solubilized with 1% DM and subjected to BN-PAGE